American Mineralogist, Volume 104, pages 1526–1529, 2019

LETTER

Single-crystal elasticity of iron-bearing phase E and seismic detection of water in Earth's upper mantle

NICCOLÒ SATTA[1,*], HAUKE MARQUARDT[2], ALEXANDER KURNOSOV[1], JOHANNES BUCHEN[3], TAKAAKI KAWAZOE[4], CATHERINE MCCAMMON[1], AND TIZIANA BOFFA BALLARAN[1]

[1]Bayerisches Geoinstitut, Universität Bayreuth, 95440 Bayreuth, Germany
[2]Department of Earth Sciences, University of Oxford, Oxford OX1 3AN, U.K.
[3]Seismological Laboratory, California Institute of Technology, Pasadena, California 91125, U.S.A.
[4]Department of Earth and Planetary Systems Science, Hiroshima University, Hiroshima 739-8526, Japan

ABSTRACT

The elastic properties of $Mg_{2.12(2)}Fe_{0.21(2)}Ni_{0.01}Si_{1.15(1)}O_6H_{2.67(8)}$ phase E single crystals with $Fe^{3+}/\Sigma Fe = 0.25(3)$ have been determined by Brillouin spectroscopy at ambient conditions. We find that that the elasticity of iron-bearing phase E is described by the six independent stiffness tensor components (all in units of GPa): $C_{11} = 192.2(6)$, $C_{12} = 56.4(8)$, $C_{13} = 43.5(8)$, $C_{14} = -4.3(3)$, $C_{33} = 192.1(7)$, $C_{44} = 46.4(3)$. The Voigt-Reuss-Hill averages of bulk and shear moduli are 95.9(4) and 59.6(2) GPa, respectively. The aggregate velocities of iron-bearing phase E are $v_P = 7.60(2)$ and $v_S = 4.43(1)$ km/s, markedly lower than those of major mantle minerals at ambient conditions. Modeling based on our results suggests that the presence of iron-bearing phase E may reduce the sound wave velocities in upper mantle and transition zone rocks, making it a possible target for future seismological investigations aiming to map hydration in subducting slabs.

Keywords: DHMS, phase E, Brillouin spectroscopy, elasticity

INTRODUCTION

Knowledge of the abundance and distribution of H_2O ("water") in the upper mantle is important for quantifying Earth's deep water cycle and improving our understanding of dynamic mantle processes, including deep earthquakes and magmatism (Schmidt and Poli 1998; Hacker et al. 2003). Subduction of oceanic lithosphere (slabs) is the main mechanism to transport water into Earth's interior. The alteration of oceanic lithosphere leads to the formation of OH-rich serpentine minerals at the expense of olivine and pyroxene. Upon subduction, water might be successively released as a free fluid at ~200 km depth after the breakdown of serpentine (Ulmer and Trommsdorff 1995). Along a cold geotherm typical of subducting slabs, however, water can be stored in dense hydrous magnesium silicate (DHMS) phases and transported to greater depths (e.g., Nishi et al. 2014). Phase E is a member of the DHMS group; it crystallizes in the $R\bar{3}m$ space group and is non-stoichiometric (Kudoh et al. 1993). The crystal structure of phase E is characterized by brucite-like sheets $[(Mg,Fe)(OH)_2]$ of edge-sharing polyhedra that are stacked along the *c*-axis and connected by randomly occupied interlayer cation sites (Supplemental[1] Fig. S1). Commonly, Si^{4+} occupies the tetrahedrally coordinated cation sites (TO_4), while Mg^{2+} and Fe^{2+}/Fe^{3+} occupy the octahedrally coordinated sites (MO_6). All of these structural aspects lead to a very low density of phase E and allow up to ~18 wt% of water to be incorporated in the crystal structure (Crichton and Ross 2000). Since phase E has been found to be stable at temperatures up to 1200 °C at 13.5 GPa (Komabayashi et al. 2005), it could act as an important carrier of water into the deep mantle. Based on high-pressure X-ray diffraction (XRD) measurements, Shieh et al. (2000) reported a relatively low isothermal bulk modulus K_{0T} of 93(4) GPa for iron-free phase E that was later confirmed for an iron-bearing single crystal of phase E (Crichton and Ross 2000). The low bulk modulus of phase E could cause a detectable seismic signature in subducted slabs since it could lead to comparably low compressional wave velocities. However, no information on the shear modulus and the elastic anisotropy of phase E has been previously reported, hampering the interpretation of seismological observations. In this study, we conducted Brillouin scattering measurements on iron-bearing phase E single crystals at ambient conditions to quantify the compressional and shear wave velocities as well as the elastic anisotropy of phase E.

MATERIALS AND METHODS

San Carlos olivine powder was loaded into a platinum capsule together with distilled water. Phase E crystals were synthesized at 14 GPa and 1100 °C for 3 h in a multi-anvil apparatus at Bayerisches Geoinstitut (Germany). The chemical compositions of five grains were determined using an electron microprobe (JEOL JXA-8200) operated at a low beam current (5 nA) and with a defocused beam (10 μm in diameter) to minimize any possible damage to the samples. The average major element concentrations based on 139 analyzed points are 7.7(4) wt% FeO, 43.8(3) wt% MgO, 35.4(3) wt% SiO_2, and 0.3(1) wt% NiO. To determine the $Fe^{3+}/\Sigma Fe$ ratio by Mössbauer spectroscopy, five crystals were glued together on a plastic holder to form a wide circular mosaic aggregate with a diameter of 600 μm and a thickness of 400 μm. A Mössbauer spectrum (Supplemental[1] Fig. S2) was collected in transmission mode using a ^{57}Co point source. A least-square fitting procedure of Lorentzian functions implemented in the software MossA (Prescher et al. 2012) was used to fit the acquired spectrum. A model was employed using three quadrupole doublets. The center shifts (CS) of the doublets are located at 0.33(3) mm/s for CS_1, 1.08(1) mm/s for CS_2, and 1.10(2) mm/s for CS_3 when using a velocity scale calibrated using α-Fe (former National Bureau of Standards material no. 1541). The spectral components are interpreted to arise from both octahedrally coordinated ferric (CS_1) and ferrous

* E-mail: niccolo.satta@uni-bayreuth.de; Orcid 0000-0003-0397-6511

(CS_2, CS_3) iron. Based on the relative areas, a $Fe^{3+}/\Sigma Fe$ ratio of 0.25(3) has been determined. The resulting mineral formula of the studied phase E samples based on six oxygen atoms per formula unit (Kanzaki 1991) is $Mg_{2.12(2)}Fe^{2+}_{0.16(1)}Fe^{3+}_{0.05(1)}Ni_{0.01}Si_{1.15(1)}O_6H_{2.67(8)}$, where the H_2O content of 12.4(4) wt% has been estimated from the deviation of the sum of the analyzed oxides from 100%. Two optically clear single crystals were selected for Brillouin spectroscopy, oriented on a four-circle Eulerian cradle using XRD, and then double-side polished to a thickness of about 20 μm. Single-crystal XRD and Brillouin scattering measurements were conducted at ambient conditions using the combined system at the Bayerisches Geoinstitut (Trots et al. 2011; Kurnosov et al. 2017). Single-crystal diffraction experiments were performed employing a Mo$K\alpha$ X-ray flux generated by a rotating anode source operating at 50 kV and 40 mA. Diffracted X-rays were detected by a scintillation point detector. X-ray reflection profiles were recorded using the 8-position centering method (King and Finger 1979) and analyzed with the SINGLE software (Angel and Finger 2011) to correct for imperfect crystal centering. The refined unit-cell parameters obtained from a total of 15 centered reflections were a = 2.9748(6) Å, c = 13.8873(5) Å, v = 106.43(4) Å^3. A density of 3.04(1) g/cm^3 was calculated from the combination of the XRD results and the chemical analysis. Platelet normal vectors for crystal 1 and crystal 2 were found to be (0.84, –0.54, –0.01) and (0.11, –0.5, 0.86), respectively, in a Cartesian coordinate system where the Y-axis is parallel to the b*-axis and the Z-axis is parallel to the c-axis. Brillouin spectroscopy experiments were carried out using a solid-state Nd:YVO_4 laser source with a wavelength of λ = 532 nm. Brillouin frequency shifts were quantified using a six-pass Fabry-Perot interferometer (Lindsay et al. 1981) combined with an avalanche photodiode detector. All measurements were conducted using a symmetric forward scattering geometry (Whitfield et al. 1976; Speziale et al. 2014) with a measured external scattering angle (θ) of 80.8° calibrated using a silica reference glass. Experimentally determined frequency shifts (Δω) were converted to velocities (v) using the equation

$$v = \frac{\Delta\omega\lambda}{2\sin(\theta/2)}$$

where λ is the laser wavelength in air. We inverted experimentally measured sound wave velocities (v) together with crystallographic orientations and density to find the weighted nonlinear best fit to the Christoffel equation (Haussühl 2008) and to constrain all six independent components of the stiffness tensor (C_{ij}). Experimentally measured sound wave velocities as well as direction cosines and modeled velocities are given in Supplemental[1] Tables S1 and S2. We calculated the adiabatic bulk (K_S) and shear (G) moduli from the C_{ij} values using the Voigt-Reuss-Hill averaging procedure (Hill 1952; Watt et al. 1976).

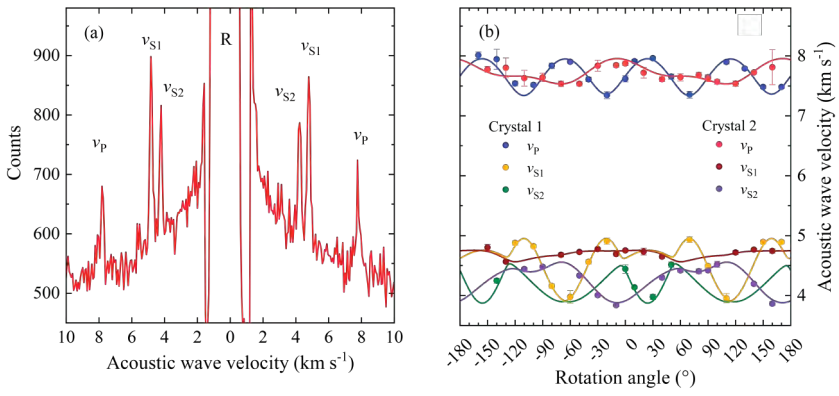

▲ **Figure 1.** (**a**) Representative Brillouin spectrum of iron-bearing phase E. Labeled peaks arise from inelastic anti-Stokes and Stokes scattering by quasi-longitudinal (v_P), quasi-transversal fast (v_{S1}), and quasi-transversal slow (v_{S2}) acoustic modes. The peak of elastically scattered light is marked with R. (**b**) Experimentally measured (filled circles) and calculated (solid curves) acoustic wave velocities as a function of the rotation angle. (Color online.)

Table 1. Components of the single-crystal stiffness tensor and Voigt and Reuss elastic moduli for a polycrystalline aggregate of phase E

C_{ij}	Value (GPa)	Parameters	Value (GPa)
C_{11}	192.2(6)	K_{Voigt}	95.9(3)
C_{33}	192.1(7)	G_{Voigt}	61.0(2)
C_{44}	46.4(3)	K_{Reuss}	95.8(4)
C_{12}	56.4(8)	G_{Reuss}	58.1(2)
C_{13}	43.5(8)	K_S	95.9(4)
C_{14}	–4.3(3)	G	59.6(2)

Notes: K_S and G were calculated using the Voigt-Reuss-Hill averaging scheme. Uncertainties on Hill averaged values have been calculated as the arithmetic mean between Voigt and Reuss bound uncertainties.

Results and Discussion

A representative Brillouin spectrum of iron-bearing phase E is shown in Figure 1a. Figure 1b shows the observed angular dispersion of acoustic wave velocities for both crystals together with computed wave velocities using the Christoffel equation and the best-fit C_{ij} values. All measured velocity data are provided in Supplemental[1] Tables S1 and S2, while the best-fit elastic parameters are given in Table 1.

C_{11} and C_{33} show the same values within uncertainties, indicating that the stiffnesses along the a-axis and c-axis are similar. The elastic shear components C_{66} and C_{44} [where $C_{66} = (C_{11} - C_{12})/2$ and $C_{44} = C_{55}$] show different values, where C_{44} is ~30% smaller than C_{66}. The low value of C_{44} (and C_{55}) may be related to the low cation occupancies of the interlayer TO_4 and MO_6 polyhedra, which translate to a low resistance to shear stress in planes perpendicular to the structural layering. On the other hand, the edge-sharing polyhedra in the brucite-like sheets may be responsible for the relatively high value of C_{66}. Elastic wave velocities propagating in a phase E single crystal have been computed using the C_{ij} values as reported in Table 1 to investigate acoustic wave anisotropy (Supplemental[1] Fig. S3). The shear wave polarization anisotropy (in percentage), $A_{vs} = 200(v_{S1} - v_{S2})/(v_{S1} + v_{S2})$, reaches its maximum of ~20% along [100] in the basal plane. The fastest compressional waves propagate in the basal plane with a velocity of 7.96 km/s (v_{Pmax}) while the slowest wave propagates with 7.25 km/s (v_{Pmin}) along [0.61, 0.35, 0.71], i.e., in a direction between the basal plane and the c-axis. The maximum longitudinal anisotropy (in percentage) is ~9%, calculated as $A_{vp} = 200 \times (v_{Pmax} - v_{Pmin})/(v_{Pmax} + v_{Pmin})$.

Implications

Based on our single-crystal measurements on phase E, we derived aggregate compressional and shear sound wave velocities of v_P = 7.60(2) and v_S = 4.43(1) km/s at ambient conditions. These velocities are significantly lower than the sound wave velocities of other mantle minerals that are predicted to be stable along with phase E in upper mantle and transition zone rocks. A comparison among selected minerals is given in Supplemental[1] Table S3.

To estimate the effect of iron-bearing phase E on seismic velocities in subducted rocks, we used the data summarized in Supplemental[1] Table S3 to calculate isotropic aggregate velocities at ambient conditions for three different phase assemblages (phase E-bearing, hydrous, and dry). We calculated the elastic moduli of these

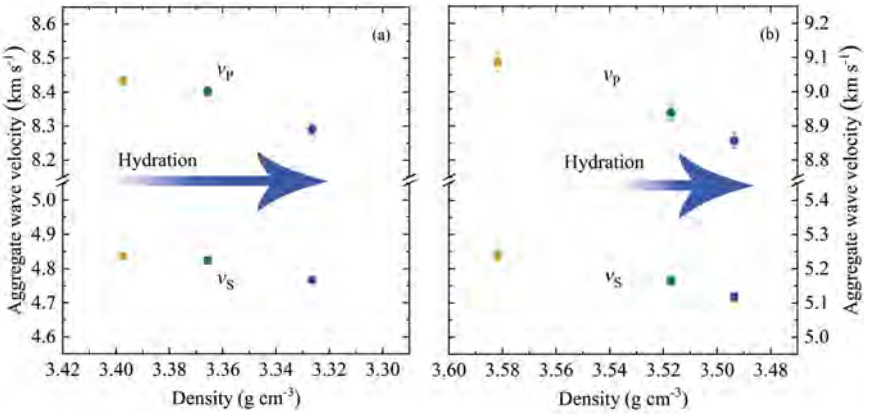

►**FIGURE 2.** Aggregate wave velocities of dry, hydrous, and phase E-bearing upper mantle (**a**) and transition zone (**b**) peridotites at ambient conditions as a function of density. Circles and squares refer to v_P and v_S, respectively. Dry, hydrous, and phase E-bearing assemblage velocities are in yellow, green, and blue colors, respectively.

assemblages using the arithmetic mean (Hill-average) of their Voigt M_V and Reuss M_R bounds, described as:

$$M_V = \sum_{i=1}^{N} M_i f_i \text{ and } 1/M_R = \sum_{i=1}^{N} f_i / M_i.$$

Here, N is the number of different mineral phases in the assemblage and f_i and M_i are the volume fractions and elastic moduli of the i-th constituent (Avseth et al. 2010), respectively. The modeled assemblages represent various stages of hydration of a cold slab of a peridotitic composition and are expected to form at conditions of the shallow transition zone (TZ) and the lowermost upper mantle (UM) just above the 410 km seismic discontinuity. The compositions of both the TZ and UM phase E-bearing assemblages are based on those given by Ohtani et al. (2004). Phase volume fractions of the employed TZ and UM assemblages as well as their acoustic velocities are listed in Supplemental[1] Table S4.

To compare velocities in hydrous (no phase E) and dry assemblages, we fixed the mineral volume fractions in dry and hydrous assemblages and only changed the hydration state of wadsleyite or olivine. For hydrous, phase E-bearing assemblages, we assume phase E to form at the expense of either hydrous wadsleyite or olivine. This is consistent with previous findings that water-saturated conditions are likely required for phase E formation in the presence of wadsleyite (Frost 1999). Furthermore, we assumed that the Mg/Fe ratio in both wadsleyite and olivine does not change once phase E is formed.

Our modeling shows that hydration and the presence of phase E in isotropic aggregates substantially reduce propagation velocities of both compressional and shear waves at ambient conditions (Fig. 2). For example, the here-considered UM phase E-bearing assemblage exhibits a reduction of 2% and 1.8% for

$$v_P = \sqrt{\frac{K_S + \frac{4}{3}G}{\rho}} \text{ and } v_S = \sqrt{\frac{G}{\rho}}$$

with respect to the dry UM assemblage (Fig. 2a). Comparison among different UM assemblages shows that hydration of olivine reduces v_P and v_S values of a dry UM assemblage by only about 0.5 and 0.3%, respectively, showing that phase E is the primary source of seismic wave speed reductions in our models. Similarly, the modeled TZ phase E-bearing assemblage is characterized by 2.5 and 2.4% slower velocities for isotropic v_P and v_S compared to the dry TZ assemblage (Fig. 2b). It has been shown experimentally that the effect of hydration on the sound wave velocities of olivine, wadsleyite, and ringwoodite significantly decreases with pressure, possibly making hydration of wadsleyite and ringwoodite invisible to seismology (Mao et al. 2010; Buchen et al. 2018; Schulze et al. 2018). The presence of phase E-bearing assemblages in cold subducting slabs, instead, might lead to a seismologically detectable reduction of seismic wave velocities, unless phase E exhibits a strong velocity increase with pressure. To evaluate the effect of pressure on phase E elasticity, we combined the here-derived ambient-pressure elastic moduli with previously published high-pressure XRD data. Previous compression studies reported different pressure derivatives of the bulk modulus (K_0') of 7.3(2) (Crichton and Ross 2000) and 5(1) (Shieh et al. 2000). We re-evaluated the previous data sets independently by fitting the reported high-pressure unit-cell volumes to a third-order Birch Murnaghan equation of state using EoSFit7c (Angel et al. 2014). Our re-evaluation of the previous XRD data (Supplemental[1] Fig. S4) shows that both previous works are consistent with K_0' ~7. Angel et al. (2001) argued that polyhedral edge-sharing, which is characteristic of DHMS phase crystal structures, controls their compression mechanism. According to the authors, the crystal structures of DHMS phases can accommodate compression by shortening of cation-oxygen bonds and/or through a deformation of the polyhedra. Among the DHMS, phase A has a density most similar to phase E and comparably low bulk and shear moduli, K_S = 106(1) GPa; G = 61 GPa (Sanchez-Valle et al. 2006, 2008). Other DHMS phases such as superhydrous phase B (Rosa et al. 2015) and phase D (Rosa et al. 2013) have more dense-packed structures and both their elastic moduli and pressure derivatives differ substantially from those of phase E. Therefore, we assume that the shear modulus of phase E shows a similar response to compression as the one of phase A. Consequently, we used the pressure derivative of the shear modulus of iron-bearing phase A, G' = 1.8 (Sanchez-Valle et al. 2008) together with a K_0' of 7.1, consistent with the re-evaluated compression studies of Crichton and Ross (2000) and Shieh et al. (2000) on phase E, to compute sound wave velocities of phase E at mantle pressures. We found that at 13 GPa and 300 K, phase E will have compressional and shear wave velocities of 7.33 and 4.88 km/s, respectively, which are about 8% and 16% lower compared to hydrous wadsleyite at the same pressure (Mao et al. 2011). Phase E might, therefore, be

a better indicator to map hydration in the shallow transition zone using seismology than the volumetrically dominant mineral wadsleyite. Future high-pressure and high-temperature experimental investigations on the elastic properties of phase E, including its high-pressure shear modulus, are needed to precisely determine how varying abundances of phase E in both randomly distributed and textured aggregates may affect the propagation of seismic waves in hydrous subducted slabs.

Acknowledgments and Funding

We thank R. Njul for polishing the crystal platelets. This research was supported through the project "GeoMaX" funded under the Emmy-Noether Program of the German Science Foundation DFG (MA4534/3-1) as well as the International Research Training Group "Deep Earth Volatile Cycles" (GRK 2156/1). H. Marquardt acknowledges support from the Bavarian Academy of Sciences. N. Satta thanks S. Speziale for his suggestions on Brillouin scattering measurements.

References cited

Angel, R.J., and Finger, L.W. (2011) SINGLE: a program to control single-crystal diffractometers. Journal of Applied Crystallography, 44(1), 247–251.

Angel, R.J., Frost, D.J., Ross, N.L., and Hemley, R. (2001) Stabilities and equations of state of dense hydrous magnesium silicates. Physics of the Earth and Planetary Interiors, 127(1-4), 181–196.

Angel, R.J., Alvaro, M., and Gonzalez-Platas, J. (2014) EosFit7c and a Fortran module (library) for equation of state calculations. Zeitschrift für Kristallographie—Crystalline Materials, 229(5), 405–419.

Avseth, P., Mukerji, T., and Mavko, G. (2010) Quantitative Seismic Interpretation: Applying Rock Physics Tools to Reduce Interpretation Risk. Cambridge.

Buchen, J., Marquardt, H., Speziale, S., Kawazoe, T., Boffa-Ballaran, T., Kurnosov, A. (2018) High-pressure single-crystal elasticity of wadsleyite and the seismic signature of water in the shallow transition zone. Earth and Planetary Science Letters, 498, 77–87.

Collins, M.D., and Brown, J.M. (1998) Elasticity of an upper mantle clinopyroxene. Physics and Chemistry of Minerals, 26, 7–13.

Crichton, W.A., and Ross, N.L. (2000) Equation of state of phase E. Mineralogical Magazine, 424, 561–567.

Frost, D.J. (1999) The stability of dense hydrous magnesium silicates in Earth's transition zone and lower mantle. In Y. Fei, C.M. Bertka, and B.O. Mysen, Eds., Mantle Petrology: Field Observations and High Pressure Experimentation: A Tribute to Francis R. (Joe) Boyd. The Geochemical Society, Special Publication No.6.

Hacker, B.R., Peacock, S.M., Abers, G.A., and Holloway, S.D. (2003) Subduction factory 2. Are intermediate-depth earthquakes in subducting slabs linked to metamorphic dehydration reactions? Journal of Geophysical Research: Solid Earth, 108(B1).

Haussühl, S. (2007) Physical Properties of Crystals: An Introduction. Wiley.

Hill, R. (1952) The elastic behavior of a crystalline aggregate. Proceedings of the Physical Society A, 65, 349–354.

Jacobsen, S.D., F. Jiang, Z. Mao, T.S. Duffy, J.R. Smyth, C.M. Holl, and Frost, D.J. (2009) Correction to "Effects of hydration on the elastic properties of olivine". Geophysical Research Letters, 36, L12302, doi:10.1029/2009GL038660.

Kanzaki, M. (1991) Stability of hydrous magnesium silicates in the mantle transition zone. Physics of the Earth and Planetary Interiors, 66(3-4), 307–312.

King, H.E., and Finger, L.W. (1979) Diffracted beam crystal centering and its application to high-pressure crystallography. Journal of Applied Crystallography, 12(4), 374–378.

Komabayashi, T., Omori, S., and Maruyama, S. (2005) Experimental and theoretical study of stability of dense hydrous magnesium silicates in the deep upper mantle. Physics of the Earth and Planetary Interiors, 153(4), 191–209.

Kudoh, Y., Finger, L.W., Hazen, R.M., Prewitt, C.T., Kanzaki, M., and Veblen, D.R. (1993) Phase E: A high pressure hydrous silicate with unique crystal chemistry. Physics and Chemistry of Minerals, 19(6), 357–360.

Kurnosov, A., Marquardt, H., Frost, D.J., Boffa Ballaran, T., and Ziberna, L. (2017) Evidence for a Fe^{3+}-rich pyrolitic lower mantle from (Al,Fe)-bearing bridgmanite elasticity data. Nature, 543(7646), 543.

Lindsay, S.M., Anderson, M.W., and Sandercock, J.R. (1981) Construction and alignment of a high performance multipass vernier tandem Fabry-Perot interferometer. Review of Scientific Instruments, 52(10), 1478–1486.

Mao, Z., Jacobsen, S.D., Jiang, F., Smyth, J.R., Holl, C.M., Frost, D.J., and Duffy, T.S. (2010) Velocity crossover between hydrous and anhydrous forsterite at high pressures. Earth and Planetary Science Letter, 293, 250–258.

Mao, Z., Jacobsen, S.D., Frost, D.J., McCammon, C.A., Hauri, E.H., and Duffy, T.S. (2011) Effect of hydration on the single-crystal elasticity of Fe-bearing wadsleyite to 12 GPa. American Mineralogist, 96(10), 1606–1612.

Nishi, M., Irifune, T., Tsuchiya, J., Tange, Y., Nishihara, Y., Fujino, K., and Higo, Y. (2014) Stability of hydrous silicate at high pressures and water transport to the deep lower mantle. Nature Geoscience, 7(3), 224.

Ohtani, E., Litasov, K., Hosoya, T., Kubo, T., and Kondo, T. (2004) Water transport into the deep mantle and formation of a hydrous transition zone. Physics of the Earth and Planetary Interiors, 143, 255–269.

Pamato, M.G., Kurnosov, A., Boffa Ballaran, T., Frost, D.J., Ziberna, L., Giannini, M., Speziale, S., Tkachev, S.N., Zhuravlev, K.K., and Prakapenka, V.B. (2016) Single crystal elasticity of majoritic garnets: Stagnant slabs and thermal anomalies at the base of the transition zone. Earth and Planetary Science Letters, 451, 114–124.

Prescher, C., McCammon, C., and Dubrovinsky, L. (2012) MossA: a program for analyzing energy-domain Mössbauer spectra from conventional and synchrotron sources. Journal of Applied Crystallography, 45(2), 329–331.

Rosa, A.D., Mezouar, M., Garbarino, G., Bouvier, P., Ghosh, S., Rohrbach, A., and Sanchez-Valle, C. (2013) Single-crystal equation of state of phase D to lower mantle pressures and the effect of hydration on the buoyancy of deep subducted slabs. Journal of Geophysical Research: Solid Earth, 118(12), 6124–6133.

Rosa, A.D., Sanchez-Valle, C., Wang, J., and Saikia, A. (2015) Elasticity of superhydrous phase B, seismic anomalies in cold slabs and implications for deep water transport. Physics of the Earth and Planetary Interiors, 243, 30–43.

Sanchez-Valle, C., Sinogeikin, S.V., Smyth, J.R., and Bass, J.D. (2006) Single-crystal elastic properties of dense hydrous magnesium silicate phase A. American Mineralogist, 91, 961–964.

Sanchez-Valle, C., Sinogeikin, S.V., Smyth, J.R., and Bass, J.D. (2008) Sound velocities and elasticity of DHMS phase A to high pressure and implications for seismic velocities and anisotropy in subducted slabs. Physics of the Earth and Planetary Interiors, 170(3-4), 229–239.

Schmidt, M.W., and Poli, S. (1998) Experimentally based water budgets for dehydrating slabs and consequences for arc magma generation. Earth and Planetary Science Letters, 163(1-4), 361–379.

Schulze, K., Marquardt, H., Kawazoe, T., Boffa Ballaran, T., McCammon, C., Koch-Müller, M., Kurnosov, A., and Marquardt, K. (2018) Seismically invisible water in Earth's transition zone? Earth and Planetary Science Letters, 498, 9–16.

Shieh, S.R., Mao, H.K., Konzett, J., and Hemley, R.J. (2000) In-situ high pressure X-ray diffraction of phase E to 15 GPa. American Mineralogist, 85, 765–769.

Speziale, S., Marquardt, H., and Duffy, T.S. (2014) Brillouin scattering and its application in geosciences. Spectroscopic Methods in Mineralogy and Materials Sciences, 78, 543–603.

Trots, D.M., Kurnosov, A., Vasylechko, L., Berkowski, M., Boffa Ballaran, T., and Frost, D.J. (2011) Elasticity and equation of state of $Li_2B_4O_7$. Physics and Chemistry of Minerals, 38(7), 561.

Ulmer, P., and Trommsdorff, V. (1995) Serpentine stability to mantle depths and subduction-related magmatism. Science, 268, 858–861.

Watt, J.P., Davies, G.F., and O'Connell, R.J. (1976) The elastic properties of composite materials. Reviews of Geophysics, 14(4), 541–563.

Webb, S.L. (1989) The elasticity of the upper mantle orthosilicates olivine and garnet to 3 GPa. Physics and Chemistry of Minerals, 16(7), 684–692.

Whitfield, C.H., Brody, E.M., and Bassett, W.A. (1976) Elastic moduli of NaCl by Brillouin scattering at high pressure in a diamond anvil cell. Review of Scientific Instruments, 47(8), 942–947.

Manuscript received April 19, 2019
Manuscript accepted July 8, 2019
Manuscript handled by Ian Swainson

Endnote:

[1]Deposit item AM-19-107084, Supplemental Material. Deposit items are free to all readers and found on the MSA website, via the specific issue's Table of Contents (go to http://www.minsocam.org/MSA/AmMin/TOC/2019/Oct2019_data/Oct2019_data.html).